Elia, G. *et al.* (2011). *Géotechnique* **61**, No. 7, 549–563 [**doi:** 10.1680/geot.8.P.028]

Fully coupled dynamic analysis of an earth dam

G. ELIA*, A. AMOROSI†, A. H. C. CHAN‡ and M. J. KAVVADAS§

The paper studies the seismic behaviour of an existing homogeneous earth dam using a fully coupled finite-element effective stress approach in conjunction with a recently developed multi-surface, elasto-plastic constitutive model for structured soils. The model is calibrated using laboratory test results for the embankment material and the foundation soils. The initial state variables (stress, hardening parameters) are determined by simulating a simplified geological history of the foundation soil, dam construction stages and reservoir impounding, prior to the application of the earthquake shaking at the bedrock level. The paper critically reviews the role of the constitutive model parameters, the hysteretic damping introduced by the model and the additional viscous damping parameters in the accumulation of permanent displacements and in the development and subsequent dissipation of excess pore water pressures due to the seismic loading. The analyses, carried out with reference to a set of earthquake records related to different return periods, show that the overall behaviour of the system in terms of displacements is characterised by a more enhanced deformation pattern of the downstream slope as compared with the upstream one. The large plastic strains accumulation induced throughout the shaking is followed by the development of excess pore water pressures inside the dam and the foundation deposit. Nonetheless, the results are indicative of a satisfactory dynamic performance of the dam, even when subjected to severe seismic loading conditions.

KEYWORDS: constitutive relations; dams; dynamics; earthquakes; embankments

La présente communication étudie le comportement sismique d'un barrage en terre homogène en utilisant d'une méthode entièrement couplée aux éléments finis avec le concept des contraintes effectives, conjointement avec un modèle constitutif élasto-plastique multi-surfaces pour sols structurés récemment développé. On calibre le modèle en utilisant les résultats d'essais en laboratoire pour le matériau du remblai et les sols de fondation. La détermination des variables d'état (contrainte, paramètres d'écrouissage) s'effectue en simulant l'histoire géologique simplifiée du sol de fondation, les étapes de la construction du barrage, et la retenue du bassin, préalablement à l'application des secousses sismiques au niveau de la roche mère. La communication procède à un examen critique du rôle des paramètres du modèle constitutif, de l'amortissement hystérétique introduit par le modèle, et des paramètres additionnels d'amortissement visqueux dans l'accumulation de déplacements permanents, et dans la formation et la dissipation ultérieure des pressions interstitielles dues aux charges sismiques. Les analyses, effectuées relativement à un ensemble d'enregistrements de tremblements de terre portant sur différentes périodes de retour, indiquent que le comportement général du système sur le plan des déplacements est caractérisé par une tendance de déformation renforcée de la pente en aval, par rapport à la pente en amont. L'accumulation de fortes déformations plastiques induites tout au long de la secousse sismique est suivie de la formation de pressions interstitielles excessives à l'intérieur du barrage et des dépôts de fondations. Les résultats indiquent toutefois que les performances dynamiques du barrage sont satisfaisantes, même lorsque celui-ci est soumis à des mouvements sismiques sévères.

INTRODUCTION

The stress–strain response and stability conditions of large earth embankments, such as dams and dykes, have been traditionally analysed by semi-empirical approaches or simplified numerical methods, often unsuitable for the complete comprehension of their behaviour under static and (especially) dynamic conditions. The literature reports many such analyses under static conditions using classical limit equilibrium methods (e.g. Tavenas & Leroueil, 1980; Ramalho-Ortigão *et al.*, 1983; Jardine & Hight, 1987; Baker & Leshchinsky, 2001; Hunter & Fell, 2003; Krahn, 2003) or the finite-element (FE) method (e.g. Poulos *et al.*, 1972; Penman, 1986; Pagano *et al.*, 1998, 2006; Zdravkovic *et al.*, 2002; Karstunen *et al.*, 2005; Lollino *et al.*, 2005; Karstunen *et al.*, 2006) and under dynamic conditions due to seismic actions (e.g. Seed, 1980; Makdisi & Seed, 1978; Gazetas, 1982, 1987; Seed *et al.*, 1985; Prato & Delmastro, 1987; Ambraseys & Menu, 1988; Elgamal *et al.*, 1990; Gazetas & Dakoulas, 1992; Jibson, 1993; Bardet & Davis, 1996; Crespellani *et al.*, 1998; Rathje & Bray, 2000; Paoliani, 2001). The dynamic response of earth embankments is usually analysed using pseudo-static analyses, displacement methods derived from Newmark's (1965) rigid block model, or by means of site response analyses in terms of total stresses, based on the equivalent viscoelastic approach (Schnabel *et al.*, 1972; Idriss *et al.*, 1973; Idriss & Sun, 1992).

More accurate numerical analyses of embankments under seismic loading require prediction of the development and dissipation of excess pore water pressures using fully coupled effective stress formulations. Biot's theory for solid–fluid interaction (Biot, 1941; Zienkiewicz *et al.*, 1999) is becoming increasingly popular as the theoretical basis for the dynamic analysis of geotechnical structures (e.g. Arulanandan & Scott, 1993; Meroi *et al.*, 1995; Dewoolkar *et al.*, 2001; Ghosh & Madabhushi, 2003; Burke *et al.*, 2004; Dakoulas & Gazetas, 2005; Liu & Song, 2005; Madabhushi & Zeng, 2007).

The implementation of non-linear constitutive models in numerical codes has further improved the prediction of the stress–strain response of large dams during static service

Manuscript received 28 February 2008; revised manuscript accepted 12 May 2010. Published online ahead of print 9 November 2010. Discussion on this paper closes on 1 December 2011, for further details see p. ii.

* Newcastle University, Newcastle Upon Tyne, UK.
† Technical University of Bari, Bari, Italy.
‡ University of Birmingham, Birmingham, UK.
§ National Technical University of Athens, Athens, Greece.

conditions and under seismic loading (e.g. Prevost *et al.*, 1985; Griffiths & Prevost, 1988; Indraratna *et al.*, 1992; Elgamal, 1992; Kovacevic, 1994; Ladd *et al.*, 1994; Özkan *et al.*, 1996; Naylor *et al.*, 1997; Wieland & Malla, 2002; Cascone & Rampello, 2003; Özkan *et al.*, 2006). For reliable dynamic analyses, constitutive models should include an accurate description of the stress–strain behaviour of the materials under cyclic loading.

Simple elasto-plastic constitutive models can simulate only some of the features of the cyclic behaviour of soils and are unable to reproduce the observed hysteretic energy dissipation reasonably, as they are characterised by unrealistically large yield surfaces, which result in zero or very small accumulation of plastic strain during low-strain cycles. The use of such models in dynamic FE analyses requires the superposition of, often large, fictitious viscous damping, which is difficult to quantify a priori, while its magnitude can play a crucial role on the results (Woodward & Griffiths, 1996). Furthermore, these models are unable to predict the observed significant pore water pressure build-up in the low-permeability portions of earth dams during strong earthquakes, because they usually predict small plastic strain accumulation.

Advanced constitutive models (e.g. Dafalias & Popov, 1975; Prevost, 1978; Pastor *et al.*, 1990; Kavvadas & Amorosi, 2000; Rouainia & Muir Wood, 2000) are now implemented in FE codes to simulate the early development of irreversible strains and associated excess pore water pressures, thus permitting more realistic prediction of the hysteretic dissipation, and limiting the amount of the required additional viscous damping to a low value, so that it no longer significantly influences the results. Such models have been used in the analysis of serviceability and ultimate limit states of embankments and dams under static and seismic loading conditions (e.g. Arulanandan & Scott, 1993; Elgamal *et al.*, 2002; Aydingun & Adalier, 2003; Muraleetharan *et al.*, 2004; Elia *et al.*, 2005; Sica *et al.*, 2008).

In the present work a fully coupled effective stress formulation for the solid–fluid interaction is adopted, using an FE code in conjunction with an advanced soil constitutive model, to predict the dynamic behaviour of an existing homogeneous earth dam subjected to a set of earthquake accelerograms.

The first part of the paper summarises the main features of the constitutive soil model and FE code. It also describes the geometrical and geotechnical characteristics of the dam and its foundation, the calibration of the constitutive model parameters based on the available experimental data and the characteristics of the applied seismic motions. The paper then deals with the numerical simulation of the simplified geological history of the foundation soil, followed by the dam construction stages and reservoir impounding, to evaluate the initial stress state and the values of the model internal variables prior to the application of the shaking at the bedrock level. Finally, a class A prediction of the dynamic response of the dam under several seismic motions is illustrated in terms of cumulated permanent excess pore water pressures and displacements.

SITE AND DAM CHARACTERISTICS

The dam analysed (see Fig. 1) is a homogeneous earth embankment, 48 m high, located in Puglia, south-east of Italy, along the Marana Capacciotti stream, about 13·5 km south-west of the city of Cerignola (Foggia). The embankment was built between 1970 and 1975 using compacted cohesive materials (mainly sandy and clayey silts of low plasticity) with relatively homogeneous granulometry and index properties. It has a volume of 3·71 Mm^3 and retains a reservoir with a capacity of 49 Mm^3 of water. The foundation consists of a slightly overconsolidated alluvial silt layer, 12 m thick, overlying a deep, stiff, overconsolidated silty clay stratum. Fig. 1 shows the drainage system, consisting of a sub-vertical chimney drain that discharges any seepage through the dam to a horizontal drainage gallery, and a blanket drain reaching the downstream toe of the embankment. Seepage below the embankment is prevented by a concrete diaphragm in the alluvial silt layer.

The Marana Capacciotti dam site was classified as non-seismic at the time of construction, but has been later regarded as a seismic-prone zone. In particular, the seismic hazard study recently carried out by the National Institute of Geophysics and Volcanology (INGV) for Italy predicts a peak ground acceleration of 0·275g for a return period (T_R) of 1000 years and 0·194g for a return period of 475 years at the dam site. For this reason, seismic stability assessment of the dam is now needed.

The geotechnical characteristics of the dam and foundation materials were investigated in a recent geotechnical programme, including three boreholes performed along the dam crest (boreholes S1 and S2) and the downstream slope (borehole S3) and laboratory testing of 21 undisturbed core samples (Calabresi *et al.*, 2000). The mechanical behaviour of the dam and foundation soils was explored through standard oedometer and consolidated undrained triaxial (CU-TRX) compression tests. The small-strain stiffness of the various materials was investigated by means of resonant column (RC) and bender element (BE) tests.

With regard to the cohesive soil of the dam, the results of the triaxial compression tests carried out on sample S2-C3 (borehole S2, depth 15 m) at different consolidation pressures are reported in Fig. 2 (solid line) as stress paths in the p'–q plane (where p' and q are the mean effective and deviatoric stresses, respectively) and curves of deviatoric stress against deviatoric strain (q–ε_s) and pore pressure against deviatoric strain (u–ε_s).

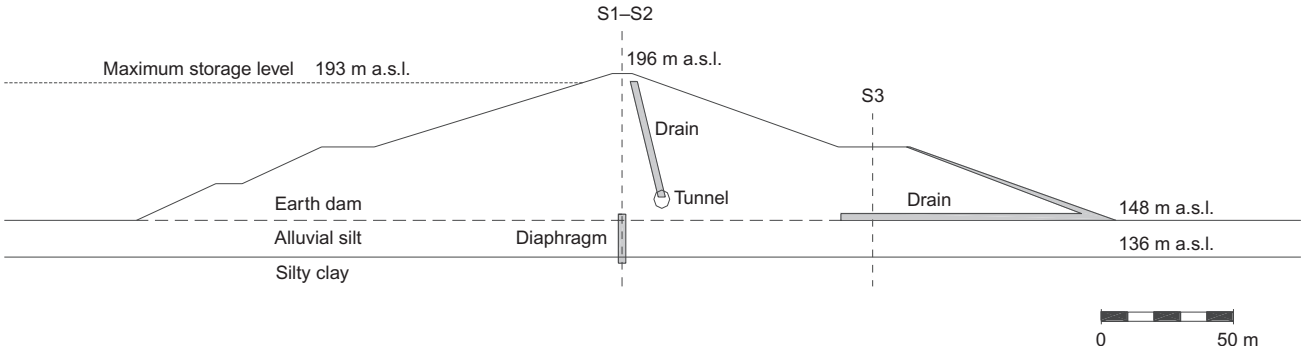

Fig. 1. Cross-section of Marana Capacciotti dam

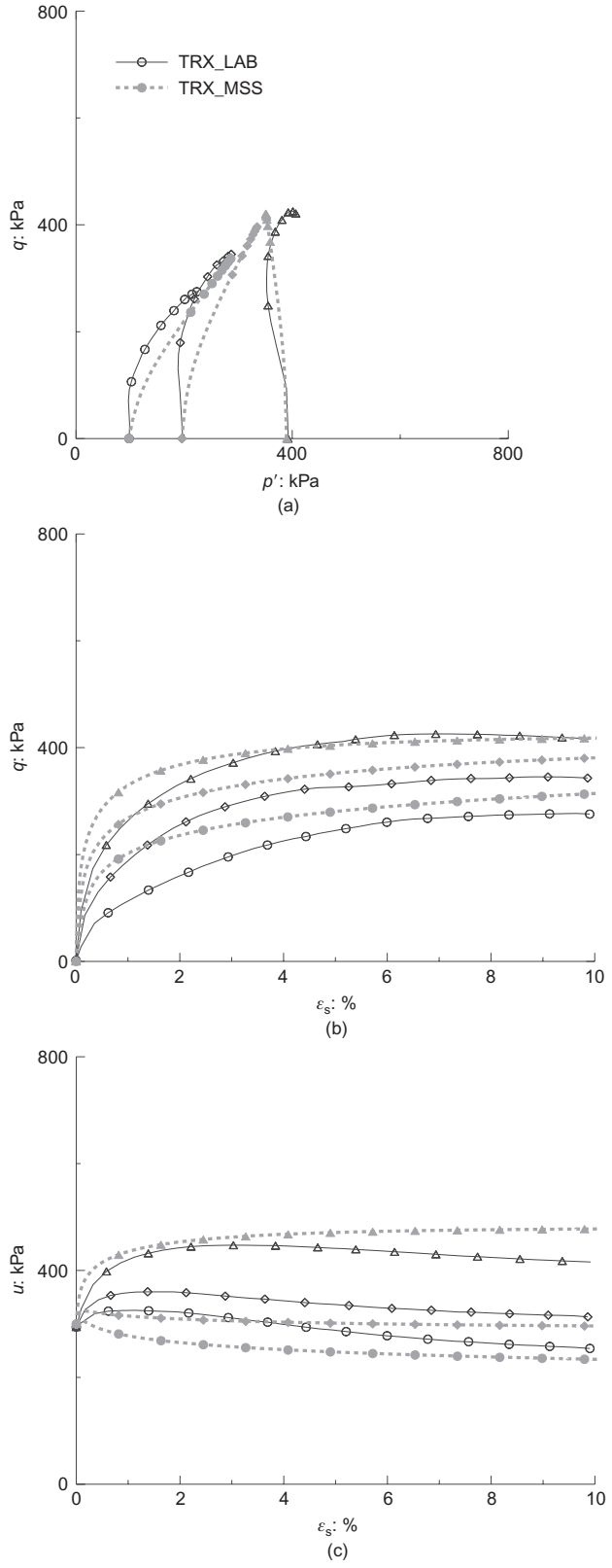

Fig. 2. Comparison between experimental results of undrained triaxial compression tests performed on dam clayey soil and computed response with MSS: (a) stress paths; (b) deviatoric stress–deviatoric strain curves; (c) pore pressure–deviatoric strain curves

Sample S1-C4 (borehole S1, depth 25 m) was tested in a resonant column apparatus. The experimental results are reported in Fig. 3 with solid lines in terms of normalised shear modulus G/G_0, damping ratio D and normalised excess pore water pressure $\Delta u/p'_0$ (p'_0 is the mean effective consolidation pressure) with cyclic shear strain amplitude γ.

For the slightly overconsolidated alluvial silt of the foundation layer, oedometer, CU-TRX and RC tests were performed on samples S1-C10, S2-C11 and S1-C11 (depths 50–55 m), respectively. The results of the triaxial tests show positive deviatoric hardening, as illustrated with solid lines in Fig. 4.

Figure 5 shows with solid lines the results of the RC test carried out on sample S1-C11 in terms of G/G_0–γ, D–γ and $\Delta u/p'_0 - \gamma$ curves.

Finally, the stress–strain behaviour of the deep overconsolidated clayey deposit was investigated using oedometer, CU-TRX and RC tests performed on sample S3-C6 (borehole S3, 2 m below the contact with the upper silty clay layer). The CU-TRX test results in the p'–q plane are reported in Fig. 6 (solid line). The observed behaviour is typical of a dilative overconsolidated cohesive soil.

The normalised curve of G/G_0–γ, the variation of damping ratio D and the normalised excess pore water pressure $\Delta u/p'_0$ with cyclic shear strain amplitude obtained from the RC test are shown in Fig. 7 with solid lines.

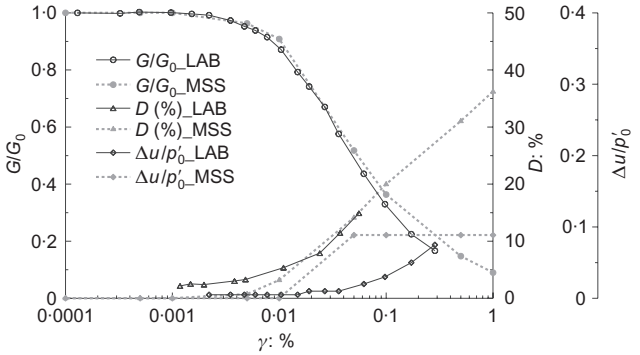

Fig. 3. Comparison between experimental results of the resonant column test performed on dam clayey soil and computed response with MSS

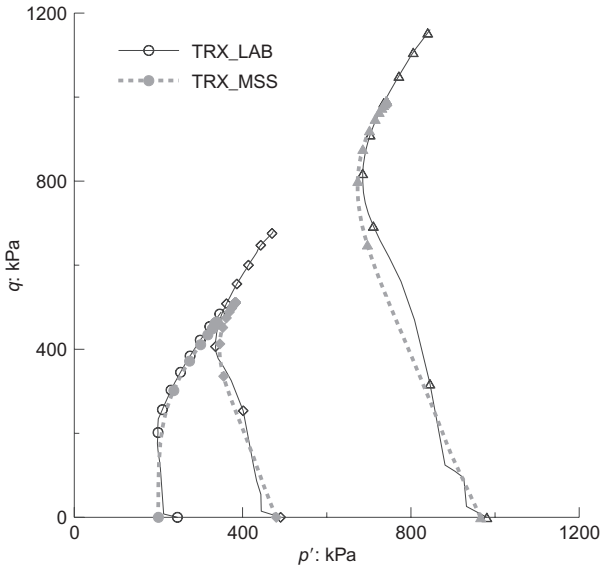

Fig. 4. Comparison between experimental results of undrained triaxial compression tests performed on alluvial silt soil and computed response with MSS in terms of stress paths

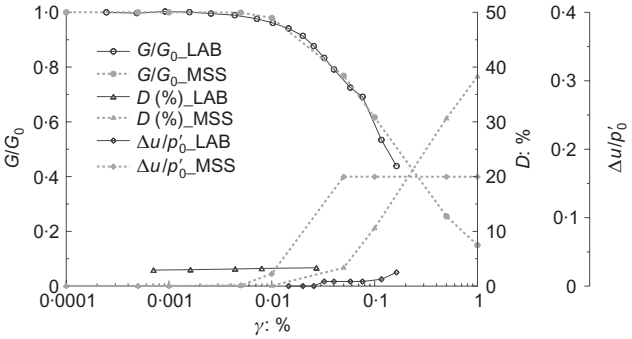

Fig. 5. Comparison between experimental results of the resonant column test performed on alluvial silt soil and computed response with MSS

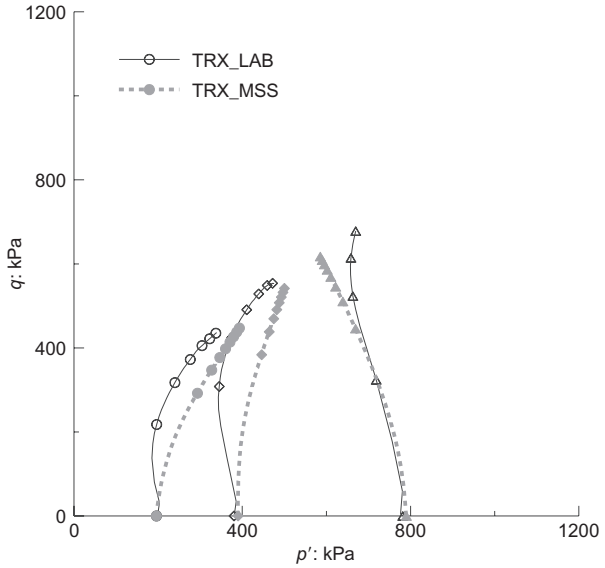

Fig. 6. Comparison between experimental results of undrained triaxial compression tests performed on silty clay soil and computed response with MSS in terms of stress paths

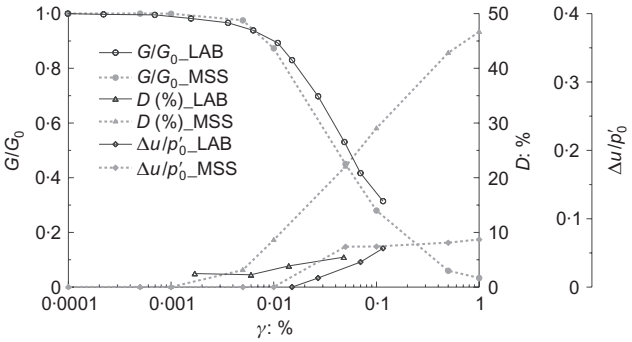

Fig. 7. Comparison between experimental results of the resonant column test performed on silty clay soil and computed response with MSS

CONSTITUTIVE MODEL AND CALIBRATION

The FE analyses employ the constitutive model for structured soils (MSS) developed by Kavvadas & Amorosi (2000), which is based on multi-surface plasticity concepts and uses two nested modified Cam-clay-like elliptical surfaces in the stress space. The model includes both isotropic and kinematic hardening. MSS can describe some of the key features of cyclic behaviour of clays, such as the decay of the shear stiffness with strain amplitude, the corresponding increase of hysteretic damping and the related accumulation of excess pore water pressure in undrained conditions (Amorosi & Kavvadas, 1999; Elia, 2004; Elia *et al.*, 2004).

The oedometer and triaxial test results mentioned in the previous section were used to calibrate the parameters for static loading conditions, while RC and BE tests were used to assess the small-strain shear stiffness profile along the dam axis and calibrate the model parameters for cyclic loading.

The virgin compressibility index λ and the swelling index κ of the dam material were determined from the results of oedometer tests. The remaining static parameters of the dam materials were determined from the results of CU-TRX tests carried out on sample S2-C3. The dashed lines in Fig. 2 show good agreement of the MSS model predictions (using the selected model parameters) with the experimental data. In the calibration process, the size of the bounding surface envelope (BSE) for each soil element was selected by considering the presumed stress history experienced by the dam material at the sampling depth, as discussed in the next section.

Numerical simulations of undrained cyclic simple shear tests were carried out in order to calibrate the model parameters controlling deviatoric destructuring, by fitting the resonant column test results performed on sample S1-C4 (Fig. 3, dashed line). The secant shear modulus for each shear strain amplitude was assessed after 500 load cycles, a number sufficient to reach steady-state condition. The calculated reduction of the normalised shear modulus G/G_0 with γ is typical of clayey soils with plasticity index 15–30% (Vucetic & Dobry, 1991), consistent with the actual embankment material. The calculated variation of the damping ratio with cyclic shear strain amplitude is in reasonable agreement with the experimental data, but shows an initial value approximately equal to zero, whereas the experimental data indicate an initial damping ratio D_0 of about 2%. This is related to the fact that the constitutive model can only simulate hysteretic damping caused by plastic strains and these are practically nil for $\gamma < 0{\cdot}001\%$ (as the associated stress paths lie within the inner plastic yield envelope, PYE), while the observed D_0 in resonant column experiments can be attributed to material viscous effects and/or the inertia of the resonant column apparatus (Meng & Rix, 2003). In order to overcome this limitation, a small amount of viscous damping of the Rayleigh type was added in the dynamic analyses of the dam.

A similar model calibration procedure was followed for the two foundation layers.

To represent the positive deviatoric isotropic hardening shown by the results of the CU-TRX tests performed on the upper slightly overconsolidated layer, negative values of the structure degradation parameters were used, in order to reproduce the characteristic dilative behaviour of the alluvial silt and the related bending towards the right of the final part of the undrained stress paths (Fig. 4, dashed line). On the other hand, the corresponding RC tests were simulated by switching off the same parameters. Fig. 5 compares the experimental data and the numerical simulations with MSS.

Finally, model calibration for the deep overconsolidated clayey deposit was carried out using the results of the oedometer, CU-TRX and RC tests performed on sample S3-C6. Fig. 6 compares the triaxial test results with the corresponding model predictions in the p'–q plane, assuming zero structure degradation.

The normalised curve of G/G_0–γ obtained from the RC test, the variation of damping D and the normalised excess pore water pressure $\Delta u/p'_0$ with cyclic shear strain amplitude were predicted using MSS, activating the deviatoric destructuring process. Fig. 7 compares the predicted curves with the corresponding test results.

It can be observed that the model tends to overestimate the damping ratio in the large-strain range, especially if the predicted D–γ curves are compared with the ones proposed by Vucetic & Dobry (1991) for clayey soils with plasticity index 15–30%. Nevertheless, this limitation of the adopted constitutive hypothesis does not affect the results of the presented dynamic simulations as the strain level effectively induced by the seismic loading in the system during all the numerical analyses is in the small to medium range (cyclic shear strain amplitude between 0·0001% and 0·1%). Stronger excitations would result in an over-damped dynamic response of the dam.

Table 1 summarises the adopted values of the model parameters for the dam material, the slightly overconsolidated foundation soil and the deep overconsolidated clayey deposit.

NUMERICAL MODEL OF THE DAM

The finite-element model

The FE analyses were performed with the computer code DIANA-SWANDYNE II, which implements the fully coupled Biot (1941) dynamic equations using the u–p simplification (Chan 1988, 1995; Zienkiewicz *et al.*, 1999). Frequency-dependent viscous damping is included via the Rayleigh damping matrix (e.g. Clough & Penzien, 1993).

The MSS constitutive model was implemented in SWANDYNE II using an explicit stress integration algorithm, based on a constant-strain sub-stepping scheme. Its predictive capabilities were extensively tested under static, consolidation and dynamic conditions for various boundary value problems (Elia, 2004).

Figure 8 shows the FE mesh used in the numerical analyses of the dam. The foundation layer extends to three times the base width of the dam in order to minimise the lateral boundary effects during the dynamic analyses. As direct measurements were not available for the dynamic shear stiffness profile of the deep silty clay stratum, a typical shear wave velocity profile was obtained using test data from similar sites located in the same region and characterised by comparable geotechnical conditions (Mucciarelli & Gallipoli, 2006). A shear wave velocity typical of a bedrock formation ($V_S = 800$ m/s) was reached within the first 30 m of the stiff clay layer and, consequently, the foundation layer was assumed to be 42 m thick (12 m of slightly overconsolidated soil underlain by 30 m of overconsolidated clay).

A mesh of 794 isoparametric quadrilateral finite elements with eight solid nodes, four fluid nodes and a 2×2 integration scheme was used. The solid nodes at the bottom of the mesh were fixed in both the vertical and horizontal directions, whereas the nodes along the lateral sides of the mesh were fixed in the horizontal direction only. Free-draining conditions were assumed for all the analyses. Fig. 9 gives the dimensions of the embankment and the foundation soils, the impervious diaphragm in the foundation, the horizontal drainage tunnel, the two drains in the embankment and the location of the nodes used in the discussion of the dynamic analyses results.

Pre-seismic static analysis of the dam

Prior to the application of the seismic loading, the initial values of the internal variables of the constitutive model (initial stress state and hardening variables) need to be determined from a static FE analysis that reproduces a simplified, though realistic, geological and stress history of the deposit, the dam construction sequence and the subsequent first reservoir impounding. In the cases studied, a simplified geological history of the clayey foundation deposit was simulated as follows. Gravity was activated in the deeper foundation layer with a hydrostatic level at a depth of 12 m from the final ground surface. A uniform vertical load of 100 kPa was applied on the horizontal surface of the deep deposit and then removed in order to simulate the overconsolidated condition of this layer. Subsequently, the size of the BSE surface in all Gauss points of the deep foundation layer was increased by 400 kPa (keeping the stress state unchanged), in order to reproduce structure generated in the stiff overconsolidated clay layer due to cementation and diagenetic processes (Kavvadas & Anagnostopoulos, 1998), and this is consistent with the size of the BSE assessed from the laboratory experimental data.

The geological history of the upper slightly overconsolidated layer was simulated by activating gravity with the water table at ground surface and then applying and removing a vertical load of 50 kPa in order to simulate the slightly overconsolidated condition of this layer.

Dam construction was then simulated by activating gravity in the four 12 m thick ideal layers of the embankment, assuming full saturation. During this phase, the hydrostatic level was maintained at ground level. As the embankment material was compacted during construction (resulting in an apparent overconsolidation), the size of the BSE in all Gauss points of the layer was increased by a factor of five while

Table 1. MSS parameters for the various materials

Material	λ	κ	$2G/K$	c	ξ	γ	ζ_q	η_q
Earth dam	0·075	0·0040	1·5	0·979	0·001	2·0	0 (monotonic) 50 (cyclic)	0 (monotonic) 200 (cyclic)
Alluvial silt	0·087	0·0030	1·5	1·090	0·001	3·0	−50 (monotonic) 0 (cyclic)	120 (monotonic) 0 (cyclic)
Silty clay	0·050	0·0008	1·5	0·990	0·001	3·0	0 (monotonic) 50 (cyclic)	0 (monotonic) 75 (cyclic)

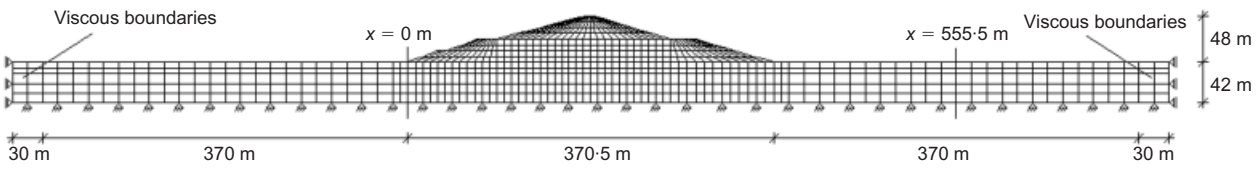

Fig. 8. Adopted FE mesh and boundary conditions

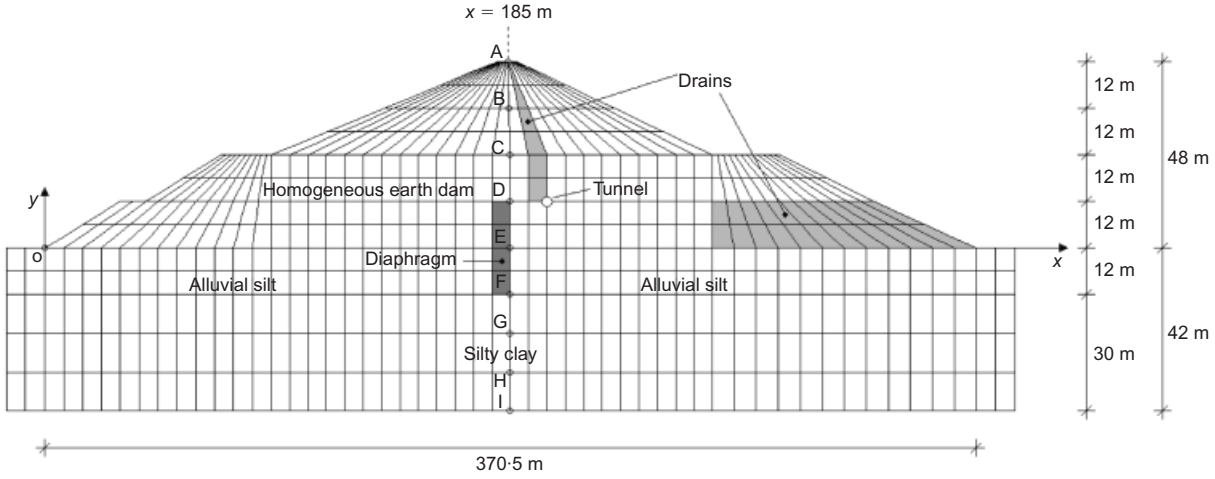

Fig. 9. Outline of FE mesh with indication of the various materials, dimensions and location of plotting nodes

keeping the stress state unchanged, in order to account for the observed increase of stiffness and strength, consistent with the behaviour observed in the laboratory tests.

Finally, reservoir impounding to the maximum serviceability conditions (elevation 190 m a.s.l.) was simulated using a coupled seepage analysis with the permeability coefficients reported in Table 2. The pore water pressure contours obtained from the seepage analysis are presented in Fig. 10: the upper part of the dam shows a maximum value of suction equal to 25 kPa at the crest.

At the end of the above simulation sequence, stress states and values of the internal variables of the constitutive model were checked for consistency with those assumed in the model calibration phase. Fig. 11(a) plots the computed overconsolidation ratio (R) profiles along the dam axis and two verticals outside the embankment: the values of R along the centreline are in good agreement with those assumed during model calibration (reported on the same figure for samples S3-C6, S2-C11 and S2-C3), confirming the consistency between laboratory-measured overconsolidation ratio, assumed values of R in the calibration stage and those obtained at the end of the static FE analyses.

Figure 11(b) plots the profile of the initial shear modulus predicted by the assumed constitutive model at the end of the static FE analyses along the axis and the corresponding test results: the computed values of G_0 are in fair agreement with the experimental results. The average initial shear modulus G_{0av} inside the dam, evaluated for each depth as the mean value of the initial shear modulus of each element of the mesh G_{0i} weighted by the element width b_i (i.e. $G_{0av} = \sum G_{0i} b_i / \sum b_i$), was divided by its maximum value at the dam base G_{0avB} and plotted against the non-dimensional depth z/H (where H is the embankment height) in Fig. 11(c): the obtained profile is close to the curve $G_{0av}/G_{0avB} = (z/H)^{2/3}$ proposed by Gazetas (1987) and based on the results of dynamic tests performed on several existing earth dams.

Table 2. Unit weight and permeability values assumed for the various materials

Material	$\overline{\gamma}$: kN/m^3	k: m/s
Earth dam	20·75	10^{-8}
Drains	20·75	10^{-6}
Diaphragm	20·75/20·40	10^{-10}
Alluvial silt	20·40	10^{-8}
Silty clay	20·50	10^{-10}

Choice of the input motions

For the evaluation of the seismic stability of the dam, three acceleration time histories were selected from a database of earthquake records (Ambraseys *et al.*, 2000) and scaled to the maximum acceleration values predicted by the INGV seismic hazard study (Gruppo di lavoro MPS, 2004) for the dam site. The average spectra of the selected time accelerograms reasonably match the response spectra proposed by INGV for the dam site for return periods of 1000 and 475 years (as shown in Fig. 12).

The peak ground accelerations predicted by the seismic hazard study correspond to input motions at 'outcropping' bedrock. In the present dynamic analyses, the scaled accelerograms were filtered to a maximum frequency of 10 Hz,

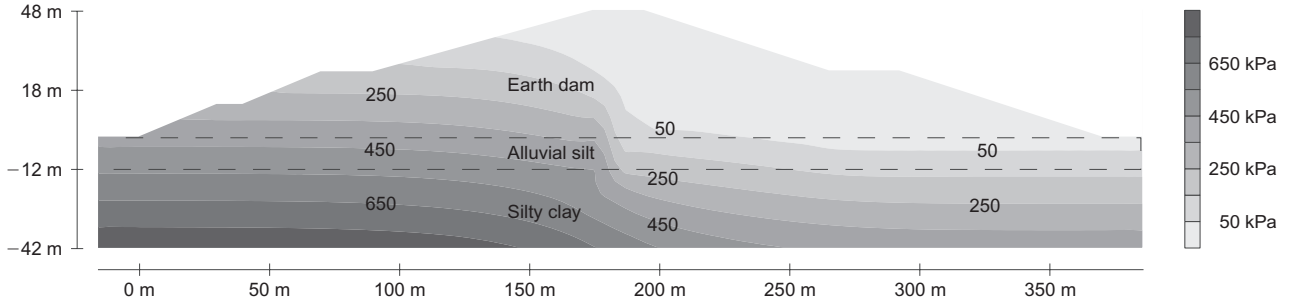

Fig. 10. Contour lines of pore water pressures at end of the seepage analysis

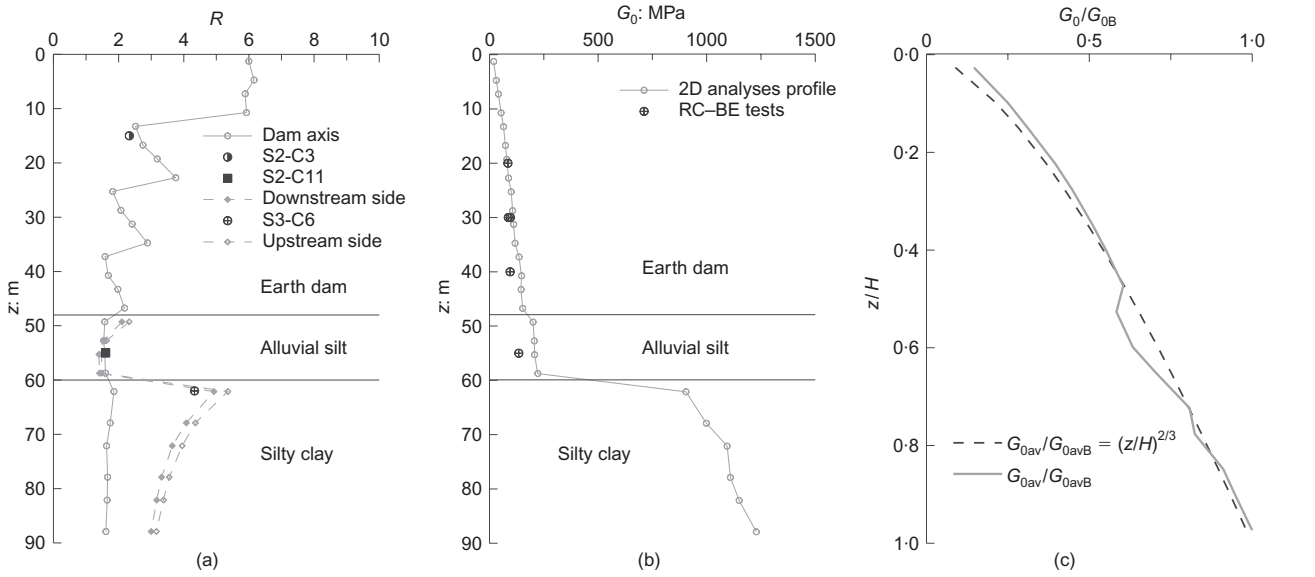

Fig. 11. Profiles with depth of: (a) overconsolidation ratio along three different verticals; (b) initial shear modulus along dam axis; (c) normalised average initial shear modulus obtained at end of static analyses of dam

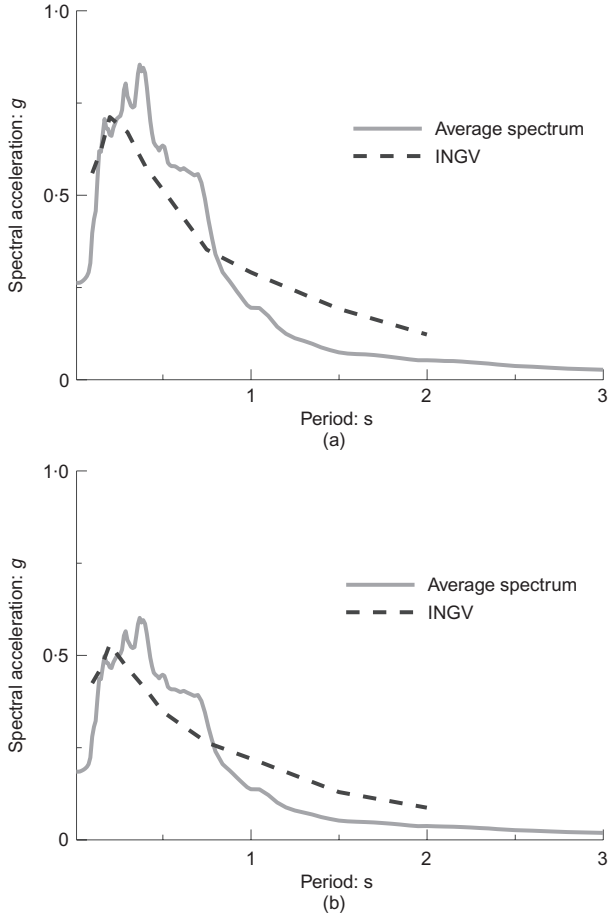

Fig. 12. Comparison between the INGV spectra predicted at dam site and average spectra of selected real accelerograms: (a) return period of 1000 years; (b) return period of 475 years

transferred to the 'base' bedrock formation through a standard de-convolution analysis (as suggested by Kwok *et al.*, 2007) and applied at the rigid base of the FE mesh. Table 3 lists the relevant characteristics of the obtained input motions.

Dynamic analyses characteristics

The dynamic behaviour of the Marana Capacciotti dam was studied applying the selected input motions to the solid nodes at the base of the mesh as prescribed horizontal displacement time histories (the nodes at the bottom of the mesh being fixed no more in both directions, but only in the vertical one). Table 4 summarises the main characteristics of each dynamic analysis performed with the FE code.

Differently from what was presented by Amorosi *et al.* (2008), the results of the fully coupled analysis of the dam subjected to the horizontal component of the accelerogram registered at Loma Prieta (Corralitos Station, Santa Cruz, USA) during the earthquake of October 1989 (characterised by a moment magnitude $M_W = 6{\cdot}9$ and a surface-wave magnitude $M_S = 7{\cdot}1$) are discussed in the following (analysis LOMA_1). The seismic motion has a peak ground acceleration of $0{\cdot}177g$, a length of 40 s and a dominant frequency of 1·39 Hz. The acceleration time history and its Fourier spectrum are plotted with thick black solid lines in Fig. 13. The dynamic response of the dam was analysed for a duration of 80 s, using a time step of 0·02 s equal to the time interval of the earthquake trace.

Time integration employed a generalised Newmark time-stepping procedure (Katona & Zienkiewicz, 1985) with parameters equal to $\beta_1 = 0{\cdot}6$ and $\beta_2 = 0{\cdot}605$ for the solid phase and $\beta_1^* = 0{\cdot}6$ for the fluid phase, in order to obtain an unconditionally stable scheme (Zienkiewicz *et al.*, 1999). The small numerical damping introduced by the time integration algorithm was not sufficient to remove all the spurious high frequencies due to the FE discretisation. As the hysteretic damping provided by the adopted constitutive model is virtually zero for cycles characterised by shear strain amplitude smaller than 0·001%, a small amount of viscous damping of the Rayleigh type was included in the dynamic simulations. In particular, a damping ratio equal to 2%, associated to the frequencies $f_1 = 0{\cdot}477$ Hz and $f_2 = 2{\cdot}385$ Hz (with $f_2 = 5f_1$, as suggested by Kwok *et al.*, 2007), was adopted in all the FE dynamic simulations. The two frequencies were selected in order to have a mean value close to the natural frequency of the system (equal to 1·21 Hz, as shown in the next section).

Moreover, viscous boundaries along the left and right sides of the foundation layer were simulated by means of two columns of elements characterised by a Rayleigh damp-

Table 3. Characteristics of the input motions used in the dynamic analyses

	Original record	T_R: years	a_{max} (outcrop): g	a_{max} (bedrock): g	f_{max}: Hz	Dominant frequency: Hz	Record length: s
A1	Corral90	1000	0·275	0·177	10	1·39	40
A2	Corral90	475	0·194	0·128	10	1·39	40
A3	AmbiestaEW	1000	0·275	0·214	10	1·49	35
A4	Ra01168EW	1000	0·275	0·148	10	2·63	40

Table 4. Dynamic analyses performed with SWANDYNE II

Name	Record	a_{max} (bedrock): g	Analysis length: s	Time step:* s
LOMA_1	A1	0·177	80	0·02
LOMA_2	A2	0·128	80	0·02
TOLMEZZO	A3	0·214	60	0·01
NOCERA	A4	0·148	60	0·01

* The time step used is the same as the time interval at which the records are measured.

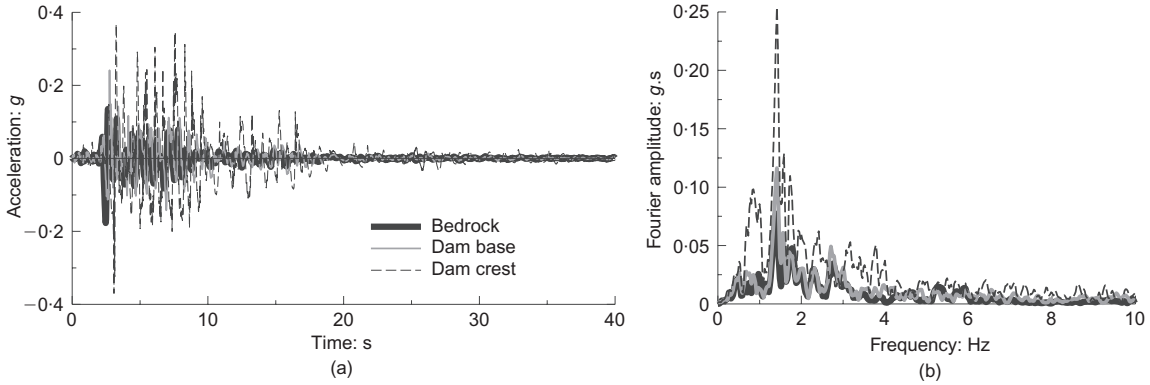

Fig. 13. Comparison between input motion applied at bedrock during analysis LOMA_1 and acceleration time histories computed along dam axis at crest of embankment and at ground surface

ing equal to 25%, in order to minimise wave reflections during the seismic action. This value, selected on the basis of a preliminary parametric study, has proved to be effective in reproducing the far-field response of the foundation layer, as discussed in the following.

DISCUSSION OF DYNAMIC ANALYSES RESULTS

Figure 13 shows, for the analysis LOMA_1, the comparison between the input motion applied at the bedrock and the acceleration time histories computed along the dam axis at the crest of the embankment and at the ground surface level. The results indicate that amplification of the seismic signal occurred essentially between the base and the crest of the embankment: the peak ground acceleration at the top of the dam is equal to 0·37g, with a magnification factor of about 2 over the peak base amplitude. The energy content of the seismic wave computed at the crest level is concentrated in the range 0–4 Hz, with a first peak of the spectral amplitude at 0·85 Hz and a second larger peak at 1·41 Hz, corresponding to the dominant frequency of the bedrock signal.

The evolution with time of the vertical and horizontal displacements (relative to the bedrock) of the nodes along the dam axis is shown in Fig. 14. The advanced constitutive assumption adopted allows the non-linear and irreversible response of the soils to be realistically simulated, leading to a final permanent horizontal displacement of the crest (node A) equal to 0·58 m and a settlement of 0·86 m, essentially due to plastic strains accumulation throughout the shaking.

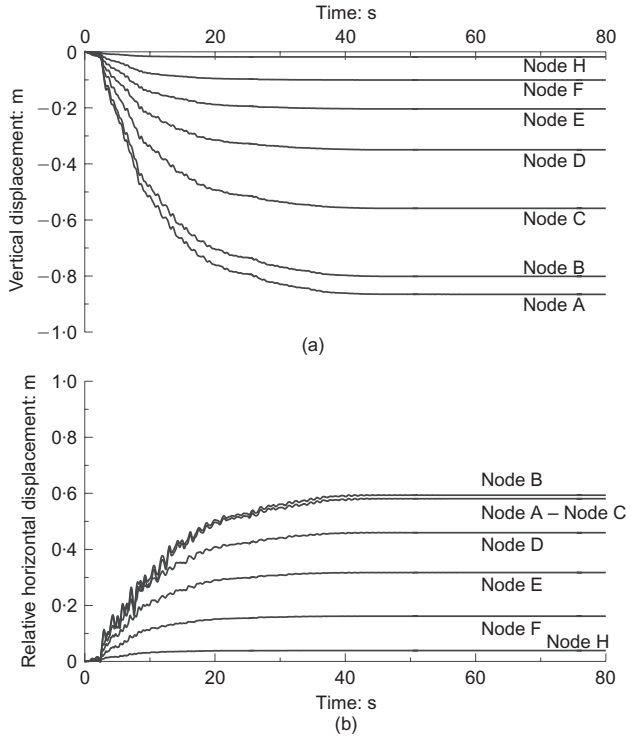

Fig. 14. Computed displacement time histories along dam axis: (a) vertical displacements; (b) relative horizontal displacements

The computed displacement time histories become constant immediately after the end of the earthquake (i.e. after 40 s) in all the monitored nodes, indicating a stable behaviour of the dam after the seismic action.

Figure 15 shows a detail of the evolution of the horizontal displacement of node A in the range 50–70 s. The low-amplitude residual oscillations of the system in the post-seismic stage of the simulation indicate that the dam and its foundation layer are oscillating around a final neutral position with a mean frequency of 1·21 Hz, representing the first natural frequency of the system.

The maximum crest settlement relative to the dam base induced by the earthquake is equal to 0·66 m, equivalent to 25% of the service freeboard (2·6 m). As the seismic action applied at the bedrock is very demanding ($T_R = 1000$ years), the results can be considered indicative of a satisfactory dynamic performance of the dam in this extreme condition.

The deformed mesh 40 s after the beginning of the shaking is shown in Fig. 16 (with a magnification factor of 10). The results indicate a larger deformation pattern of the downstream slope with respect to the upstream one, but not a failure mechanism inside the embankment.

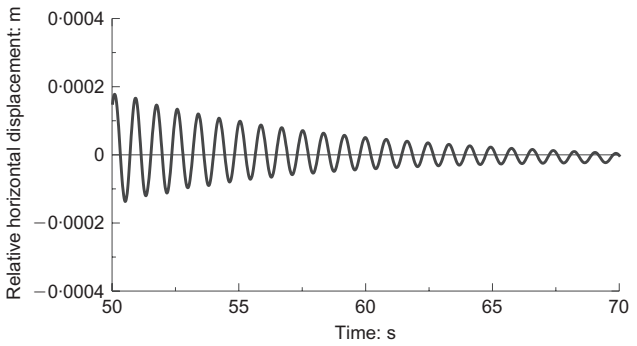

Fig. 15. Detail of horizontal displacement time history recorded at dam crest during analysis LOMA_1

The contour of excess pore water pressures at the end of the earthquake is plotted in Fig. 17. Referring to the stress state at the end of the static analyses reported in Fig. 11(a), the results can be explained as follows.

(*a*) During shaking, the portions close to the surface of the upstream and downstream slopes show an accumulation of negative excess pore water pressures, since the cohesive dam material is compacted at a 'dry of critical' state.

(*b*) The central part of the embankment, the slightly overconsolidated layer and the stiff clayey deposit below the dam are characterised by positive excess pore water pressures due to their initial 'wet of critical' state.

(*c*) The foundation deposit laying out of the dam area shows negative pore pressures related to its initial overconsolidated state, not affected by the embankment surcharge.

The dissipation of these excess pore pressures during the consolidation analysis performed at the end of the dynamic simulation (after 80 s) induces further settlements of the downstream slope of about 0·05 m.

Finally, Fig. 18 shows the contour of shear strain γ (absolute values) accumulated after 40 s, indicating the seismic-induced concentration of plastic strains propagating from the toe of the downstream slope into the slightly overconsolidated foundation layer.

Influence of Rayleigh damping

In order to highlight the effect of the additional Rayleigh damping on the results of the FE dynamic simulations, the LOMA_1 analysis was re-run, completely removing the

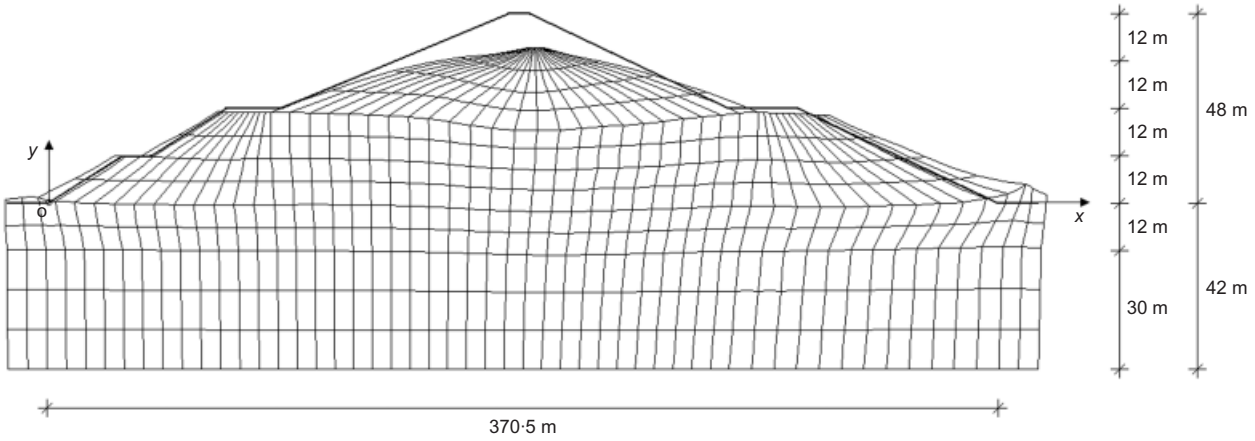

Fig. 16. Deformed mesh at end of earthquake for analysis LOMA_1 (magnification factor equal to 10)

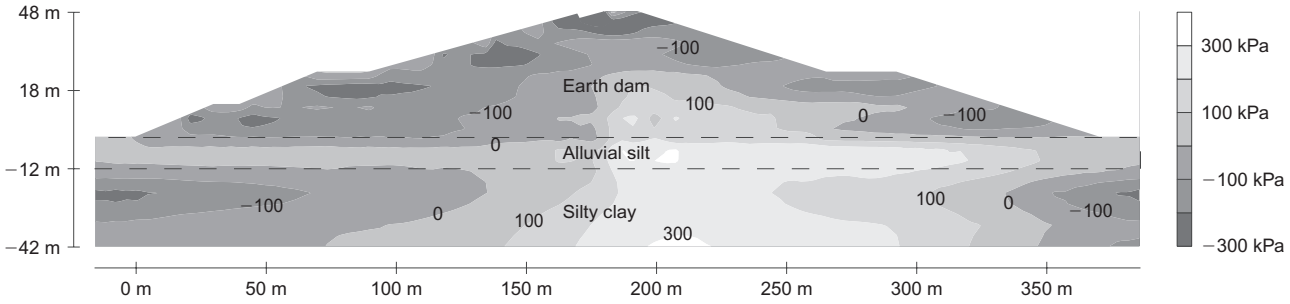

Fig. 17. Contour lines of excess pore water pressures at end of earthquake for analysis LOMA_1

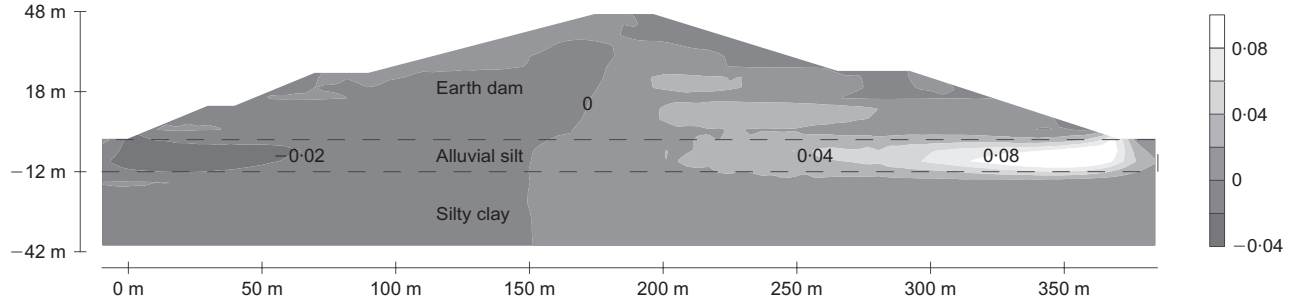

Fig. 18. Contour lines of shear strain γ at end of earthquake for analysis LOMA_1

viscous damping. The acceleration time history and its Fourier spectrum obtained at crest during this new dynamic simulation were compared with the corresponding ones relative to the LOMA_1 analysis (performed adding the 2% of Rayleigh damping). The comparison, shown in Fig. 19, indicates that the introduction of such a small amount of viscous damping provides additional dissipation essentially in the high frequencies regime (removing the spikes in the acceleration time history), although it also slightly modifies the system response in the frequency range of interest (i.e. 0–4 Hz), consistent with what was analytically proved by Hughes (1983).

Influence of input motion

The dynamic behaviour of the Marana Capacciotti dam was also studied applying to the bedrock the records A2, A3 and A4 reported in Table 3 – that is, the same Loma Prieta earthquake as used in the analysis LOMA_1, but scaled to a maximum outcropping acceleration of 0·194*g* representative of an earthquake with a return period of 475 years at the dam site (analysis LOMA_2) and the E–W horizontal components of the accelerograms registered at Tolmezzo and Nocera Umbra in Italy, with a maximum acceleration of 0·275*g* at the outcrop and a return period of 1000 years (analyses TOLMEZZO and NOCERA, respectively). The results of all the fully coupled dynamic simulations are summarised in Fig. 20 in terms of profiles with non-dimensional depth z/H of the ratio a_{max}/a_{base} between the maximum acceleration along the dam axis and at the dam base. In all the analyses, the profiles are characterised by a significant amplification of the seismic signal at the top of the dam. Moreover, the results are consistent with those obtained from the response analyses of different dams reported in the literature (Cascone & Rampello, 2003), whose envelope is indicated in Fig. 20 by the shaded area.

It is worth observing that, consistent with what was originally proposed by Seed *et al.* (1976), the FE simulation performed using a lower return period seismic record (LOMA_2) exhibits a larger amplification effect as compared with the others, even though it is characterised by the lowest energy content. This is related to the lower maximum shear strain amplitude induced in the dam by the earthquake with a return period of 475 years as compared with the 1000-year ones, thus involving higher stiffness and lower damping during the shaking. This, consequently, enhances the transmission of the high frequencies of the seismic signal and increases the amplification of the peak accelerations at the surface.

Finally, the results of the two FE dynamic analyses LOMA_1 and NOCERA, performed by applying to the bedrock two input signals characterised by distinct dominant frequencies (see Table 3), are compared in Fig. 21 in terms of acceleration time histories computed at the crest of the dam. The behaviour of the system in terms of frequency amplification is different: the energy content of the seismic wave computed during the analysis NOCERA is concentrated in the range 0–6 Hz, with a first peak of the spectral amplitude at 0·83 Hz, a second peak at 1·60 Hz and a third, larger peak at 2·69 Hz, corresponding to the dominant frequency of the bedrock signal. In this case, differently from what was discussed for the LOMA_1 case, the input signal does not shake the system close to its first natural frequency (1·21 Hz), thus producing a smaller deformation

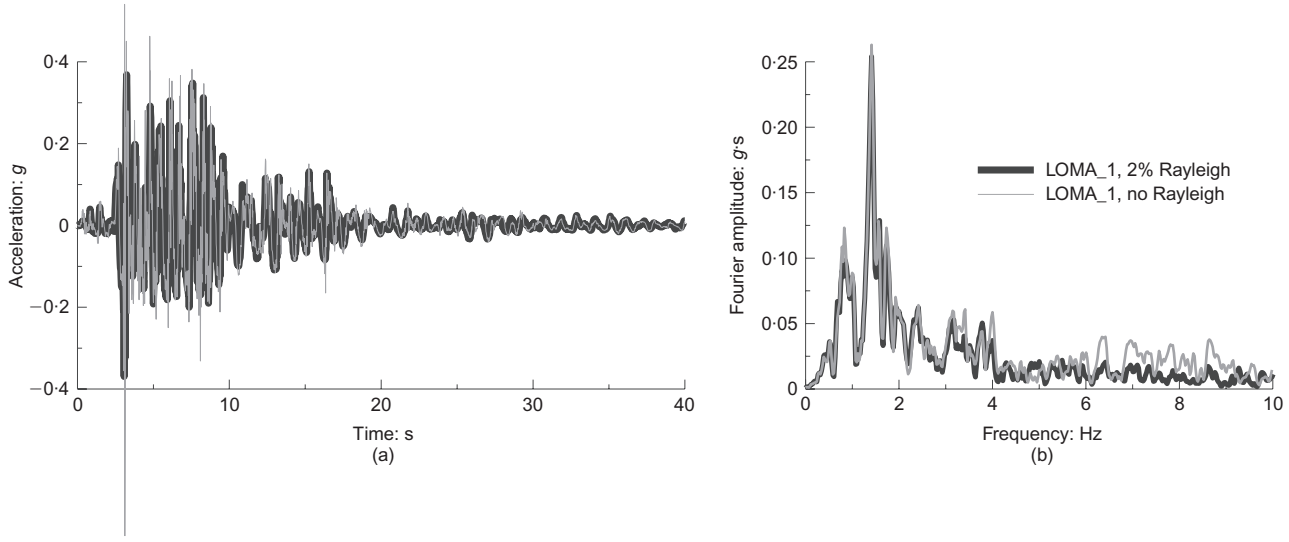

Fig. 19. Comparison between acceleration time histories computed along dam axis at crest of embankment during analysis LOMA_1 with 2% Rayleigh damping and corresponding simulation with no additional viscous damping

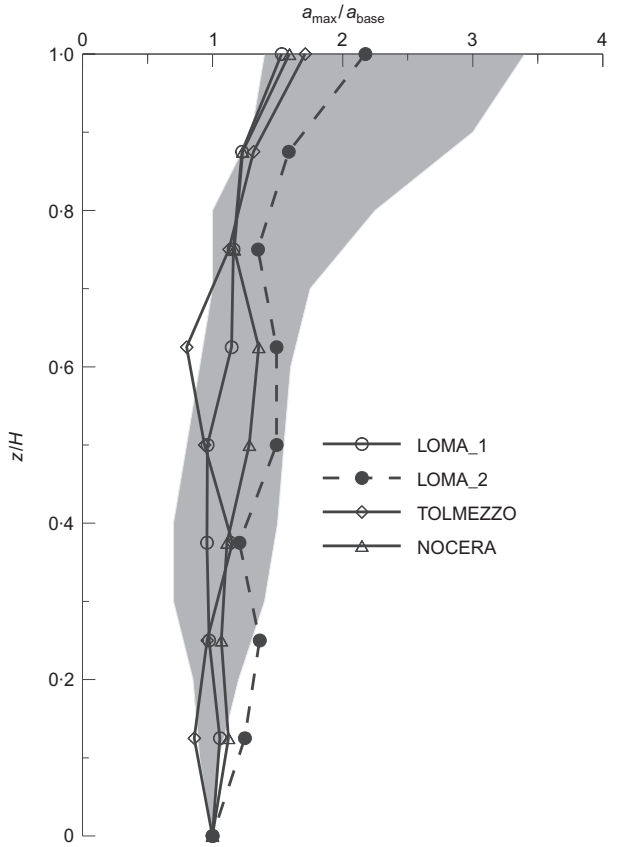

Fig. 20. Profiles of a_{max}/a_{base} computed during different 2D dynamic analyses of dam and comparison with literature results

pattern of the dam. Nevertheless, the maximum acceleration recorded at crest during this simulation, equal to 0·39*g*, is similar to that obtained in the LOMA_1 analysis (0·37*g*).

Influence of boundary conditions

As mentioned before, the far-field boundaries were simulated using two columns of elements, disposed along the left and right sides of the dam foundation layer, characterised by a high value of Rayleigh damping. In order to prove the effectiveness of this choice, the LOMA_1 analysis was re-run, assuming different boundary conditions during the dynamic simulation. In a first analysis, the two columns of viscous elements were removed (this simulation has been named 'no viscous boundaries'); in a second analysis, the tied-nodes boundaries were applied at the vertical sides of the foundation layer (named 'tied-nodes'). Moreover, the far-field response was obtained applying the input motion employed in the analysis LOMA_1 at the base of a soil column (42 m high and 5 m wide) representative of the foundation layer only (without the dam), using the tied-nodes boundary conditions. The material states and the MSS internal variables obtained at the end of the static analyses of the dam along a vertical far from both the mesh boundaries and the dam axis ($x = 555{\cdot}5$ m, Fig. 8) were used as input for this third dynamic simulation. The results of this latter analysis (named '1D response'), representative of the free-field response of the foundation layer, were compared with the ones obtained during the LOMA_1 analysis presented in the paper (named 'viscous boundaries') and during the other two additional dynamic simulations performed without viscous boundaries and employing the tied-nodes boundaries respectively. The comparison, presented in terms of Fourier spectra of the acceleration time histories recorded at ground level along the vertical at $x = 555{\cdot}5$ m, is shown in Fig. 22. The dynamic behaviour of the foundation layer obtained during the three 2D simulations is similar, regardless of the adopted boundary conditions, and results in good agreement with the far-field response, thus indicating that the adopted length of the mesh is sufficient to avoid wave reflections along the vertical boundaries during the seismic action. This also demonstrates the validity of the approach adopted in the presented dynamic simulations.

CONCLUSIONS

In this paper, the response to seismic excitation of a real homogeneous earth dam located in the southern part of Italy, overlaying a stiff natural clayey deposit, was studied using a fully coupled, effective-stress-based FE code and adopting a multi-surface elasto-plastic constitutive hypothesis to model the stress–strain behaviour of the soils involved.

The model parameters were calibrated using the available experimental data for the embankment and the foundation layers, for both static and cyclic loading conditions. Since the dynamic behaviour is substantially influenced by the existing initial static state, the internal variables of the model were initialised through appropriate static FE analyses reproducing a simplified geological history of the deposit, the following embankment construction and the subsequent reservoir impounding stages, before the application of the seismic action at the bedrock level.

The dynamic behaviour of the embankment was analysed by applying at the base of the mesh four real accelerograms

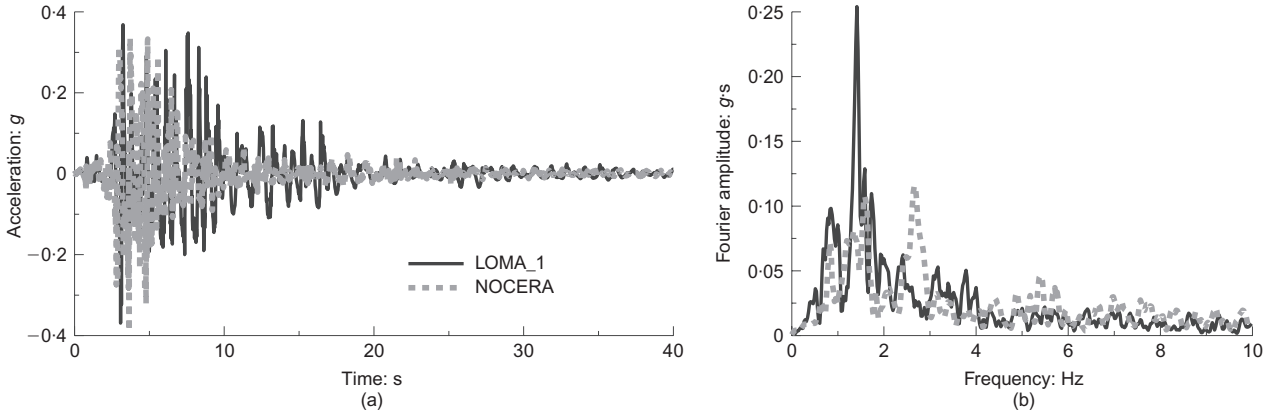

Fig. 21. Comparison between acceleration time histories computed along dam axis at crest during analyses LOMA_1 and NOCERA

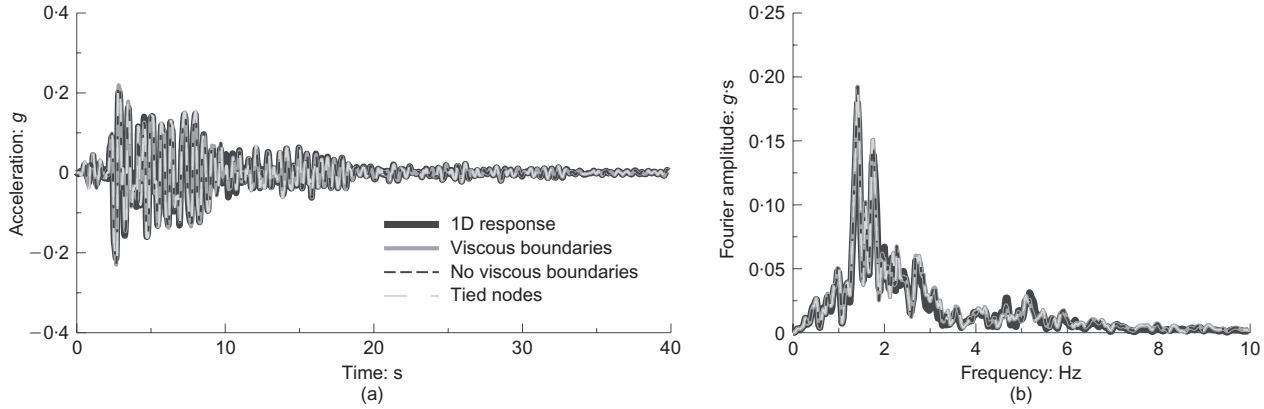

Fig. 22. Comparison between acceleration time histories computed along vertical $x = 555{\cdot}5$ m at ground surface during analyses employing different boundary conditions

representative of input motions with return periods of 1000 and 475 years at the dam site.

The resulting maximum relative crest settlement induced by the seismic loading was equal to about 25% of the service freeboard. The overall behaviour of the system in terms of displacements pointed out a greater deformation pattern of the downstream slope with respect to the upstream one, but did not give any indication of the occurrence of a failure mechanism inside the embankment. The large plastic strain accumulation induced throughout the shaking was complemented by a diffuse development of positive or negative excess pore water pressures inside the dam and the foundation deposit, depending on the initial state of the soil. The consolidation analysis performed at the end of the dynamic simulation made it possible to evaluate the amount of the additional settlements due to the dissipation of these excess pore water pressures.

When the dam was subjected to different input motions at the bedrock level, its predicted behaviour has proved to be consistent with what indicated in the literature, as follows.

(*a*) All the accelerograms characterised by the same return period of 1000 years give similar profiles of the ratio a_{max}/a_{base}, with maximum values at the crest between 1·5 and 1·7, indicating a significant amplification of the seismic signal at the top of the dam.
(*b*) During the earthquakes characterised by larger energy content, the stiffness reduction and the increase in material damping, both related to the non-linear mechanical behaviour of the soils involved in the analyses, result in a reduced amplification of the peak accelerations at the surface.
(*c*) The input signals characterised by an energy content close to the first natural frequency of the system induce larger accumulated displacements of the embankment.

The work presented in this paper has highlighted the possible benefits from the use of a fully coupled effective stress non-linear approach in the analysis of the dynamic response of large earth embankments. The advanced constitutive model and the soil skeleton–pore fluid dynamic interaction scheme adopted in the analyses has made it possible to investigate the effects of the seismic loads on the stability and serviceability conditions of the dam. As no direct displacement and pore pressure measurements during real seismic motions are available, the results of the presented FE simulations represent a class A prediction of the dynamic response of the dam in view of modern performance-based design approaches.

ACKNOWLEDGEMENTS

The research was financially supported by the Italian Ministry of University and Scientific Research (PRIN-MIUR 2005/07) and by the University Network of Seismic Engineering Laboratories (RELUIS 2005/08, Research project 6, Research line 6·3: Slope stability). The valuable comments and suggestions of the reviewers are also acknowledged.

APPENDIX: CONSTITUTIVE MODEL FORMULATION

The two characteristic surfaces of the MSS model are shown in Fig. 23. The external BSE surface is expressed by the function

$$F(\boldsymbol{\sigma}; \boldsymbol{\sigma}_K; \alpha) \equiv \frac{1}{c^2}(\boldsymbol{s} - \boldsymbol{s}_K) : (\boldsymbol{s} - \boldsymbol{s}_K) + (\sigma - \sigma_K)^2 - \alpha^2 = 0 \quad (1)$$

where $\boldsymbol{\sigma}_K$ and $\boldsymbol{s}_K$ are the isotropic and deviatoric coordinates of the centre, α is the horizontal half-axis of the ellipsoid, c is a parameter controlling the length of the vertical half-axis and the symbol ':' indicates a summation of the products. The internal yield surface PYE is described by a function similar to the BSE, but scaled by a factor ξ, as

$$f(\boldsymbol{\sigma}; \boldsymbol{\sigma}_L; \alpha) \equiv \frac{1}{c^2}(\boldsymbol{s} - \boldsymbol{s}_L) : (\boldsymbol{s} - \boldsymbol{s}_L) + (\sigma - \sigma_L)^2 - (\xi\alpha)^2 = 0 \quad (2)$$

The characteristic surfaces introduce the hardening variables (α, $\boldsymbol{\sigma}_K$, $\boldsymbol{\sigma}_L$), which control the size and the positions of their

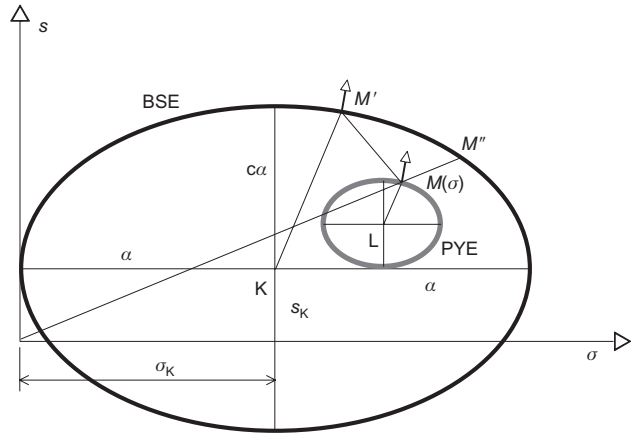

Fig. 23. Characteristic surfaces of MSS model

centres in the stress space. The evolution of the hardening variables during plastic deformation is described by the hardening rules. The model possesses both isotropic and kinematic hardening of the characteristic surfaces.

Isotropic hardening rule

In this simplified version of the model, the isotropic hardening of the BSE surface is related to the volumetric and deviatoric plastic strain increment ($\dot{\varepsilon}_v^p$, $\dot{\varepsilon}_q^p$) by the expression

$$\dot{\alpha} = \alpha\left\{\left(\frac{1+e}{\lambda-\kappa}\right)\dot{\varepsilon}_v^p + \left[-\zeta_q \cdot \exp\left(-\eta_q \varepsilon_q^p\right)\right]\dot{\varepsilon}_q^p\right\} \tag{3}$$

where λ and κ are the intrinsic compressibility parameters and ζ_q and η_q are the deviatoric structure degradation parameters. The volumetric part of the above hardening law is identical to the modified Cam-clay hardening rule, while the deviatoric component depends on the modulus of the plastic deviatoric strain increment by an exponential damage-type form, to account for deviatoric-strain-induced structure degradation.

Kinematic hardening rules

During plastic deformation, the centre K of the BSE moves along a radial path through the origin according to

$$\dot{\boldsymbol{\sigma}}_K = \frac{\dot{\alpha}}{\alpha}\boldsymbol{\sigma}_K \tag{4}$$

while the centre L of the PYE moves as follows (Fig. 23).

(*a*) For material states on the BSE (i.e. when the two surfaces are in contact at a point corresponding to the current stress state $\boldsymbol{\sigma}$), the two surfaces remain in contact, and the position of L is dictated by the position of K:

$$\frac{\boldsymbol{\sigma}-\boldsymbol{\sigma}_L}{\xi\alpha} = \frac{\boldsymbol{\sigma}-\boldsymbol{\sigma}_K}{\alpha} \Rightarrow \boldsymbol{\sigma}_L = (1-\xi)\boldsymbol{\sigma} + \xi\boldsymbol{\sigma}_K \tag{5}$$

(*b*) For material states inside the BSE, the motion of point L is such that the PYE moves towards point M', which is the conjugate of the current state M. The direction vector $\boldsymbol{\beta} = MM'$ is

$$\boldsymbol{\beta} \equiv \boldsymbol{\sigma}(M') - \boldsymbol{\sigma} = \frac{1}{\xi}(\boldsymbol{\sigma}-\boldsymbol{\sigma}_L) - (\boldsymbol{\sigma}-\boldsymbol{\sigma}_K) \tag{6}$$

and the translation of the centre L is described by the equation

$$\dot{\boldsymbol{\sigma}}_L = \frac{\dot{\alpha}}{\alpha}\boldsymbol{\sigma}_L + \dot{\mu}\cdot\boldsymbol{\beta} \tag{7}$$

The parameter $\dot{\mu}$ is determined from the consistency condition, which requires that the stress point remains on the PYE (i.e. $\dot{f} = 0$).

Flow rule

The flow rule of MSS is associated and has the standard form

$$\dot{\boldsymbol{\varepsilon}}^p = \dot{\Lambda}\frac{\partial f}{\partial \boldsymbol{\sigma}} \text{ where } \dot{\Lambda} = \frac{1}{H}\left(\frac{\partial f}{\partial \boldsymbol{\sigma}} : \dot{\boldsymbol{\sigma}}\right) \tag{8}$$

where H is the plastic modulus. For material states on the BSE, H is determined from the consistency condition, while for material states inside the BSE it is evaluated from the requirement for a continuous variation of its magnitude as the PYE approaches the BSE. This is expressed by the interpolation rule

$$H = H'' + |H''|\left\{[1-(\delta/\delta_0)]^{-\gamma^*} - 1\right\} \tag{9}$$

where H'' is the value of H at point M'' on the BSE (Fig. 23), δ is the normalised length of MM', δ_0 is the MM' length when plastic strain starts to accumulate and γ^* controls the rate of decay of the plastic modulus from $H = \infty$ upon initiation of yielding to $H = H''$ when the stress state reaches the BSE.

Elasticity

The elastic component describes the behaviour inside the PYE where deformation is by definition elastic. According to standard plasticity, strain increments consist of elastic (i.e. reversible) and plastic (i.e. irreversible) components, which can be split into volumetric and deviatoric parts as follows

$$\dot{\boldsymbol{\varepsilon}} = \dot{\boldsymbol{\varepsilon}}^e + \dot{\boldsymbol{\varepsilon}}^p \Rightarrow \dot{\varepsilon}_v = \dot{\varepsilon}_v^e + \dot{\varepsilon}_v^p \tag{10a}$$

and

$$\dot{\boldsymbol{e}} = \dot{\boldsymbol{e}}^e + \dot{\boldsymbol{e}}^p \tag{10b}$$

The elastic component of the strain increment is assumed to be linearly related to the corresponding effective stress increment via an elastic stiffness $\boldsymbol{C}^e$

$$\dot{\boldsymbol{\sigma}} = \boldsymbol{C}^e : \dot{\boldsymbol{\varepsilon}}^e \tag{11}$$

In linear isotropic elasticity, the elastic stiffness depends on two material constants, the bulk modulus K and the shear modulus G, and the stress–strain relationships are

$$\dot{\sigma} = K\dot{\varepsilon}_v^e \tag{12a}$$

$$\dot{\boldsymbol{s}} = 2G\dot{\boldsymbol{e}}^e \tag{12b}$$

In this simplified version of the model a poro-elasticity assumption is employed, which assumes that the elastic volume compressibility is linearly related to the logarithm of the mean effective stress. Therefore the model has a pressure-dependent bulk modulus given by $K = (1+e)\sigma/\kappa$, where κ is the Cam-clay compressibility parameter.

NOTATION

a_{max}	earthquake maximum acceleration
c	eccentricity of BSE and PYE
D	damping ratio
e	void ratio
$\dot{\boldsymbol{e}}$	tensorial deviatoric strain
e (superscript)	elastic component of strain
F	function of the BSE
f	function of the PYE
f_{max}	earthquake maximum frequency
G	shear modulus
H	elasto-plastic modulus
K	bulk modulus
k	permeability coefficient
M_W, M_S	moment and surface-wave magnitude
p'	mean effective stress
p'_0	mean effective consolidation pressure
p (superscript)	plastic component of strain
q	scalar stress deviator
R	overconsolidation ratio
$\boldsymbol{s}$	tensorial stress deviator
T_R	return period
u, Δu	pore and excess pore pressure
V_S	shear wave velocity
α	size of the BSE

β_1, β_2, β_1^* generalised Newmark parameters
γ cyclic shear strain amplitude
γ^* parameter controlling the variation of elasto-plastic modulus H
$\overline{\gamma}$ unit weight
$\boldsymbol{\varepsilon}$ strain tensor
ε_q scalar deviatoric strain
ε_v volumetric strain
ζ_q, η_q deviatoric structure degradation parameters
κ poro-elastic compressibility
λ intrinsic compressibility
ξ ratio of the sizes of the BSE and PYE
σ mean effective stress
$\boldsymbol{\sigma}$ effective stress tensor
σ_K coordinates of centre of BSE in the stress space
σ_L coordinates of centre of PYE in the stress space

REFERENCES

Ambraseys, N. A. & Menu, J. M. (1988). Earthquake-induced ground displacements. *Earthquake Engng and Struct. Dynam*. **16**, No. 7, 985–1006.

Ambraseys, N., Smit, P., Berardi, R., Rinaldis, D., Cotton, F. & Berge, C. (2000). *Dissemination of European Strong-Motion Data*, CD-ROM collection. Brussels: European Commission, DGXII, Science, Research and Development.

Amorosi, A. & Kavvadas, M. (1999). A plasticity-based constitutive model for natural soils: a hierarchical approach. *Proc. 3rd Eur. Conf. on Constitutive Modelling of Granular Materials, Horton, Greece*, 413–438.

Amorosi, A., Elia, G., Chan, A. C. H. & Kavvadas, M. (2008). Fully coupled dynamic analysis of a real earth dam overlaying a stiff natural clayey deposit using an advanced constitutive model. *Proc. 12th Int. Conf. of IACMAG, Goa*, 2750–2757.

Arulanandan, K. & Scott, R. F. (eds) (1993). *Proceedings of VELACS symposium*. Rotterdam: A. A. Balkema.

Aydingun, O. & Adalier, K. (2003). Numerical analysis of seismically induced liquefaction in earth embankment foundations. Part I. Benchmark model. *Can. Geotech. J.* **40**, No. 4, 753–765.

Baker, R. & Leshchinsky, D. (2001). Spatial distribution of safety factors. *J. Geotech. Geoenviron. Engng ASCE* **127**, No. 2, 135–145.

Bardet, J. P. & Davis, C. A. (1996). Performance of San Fernando dams during 1994 Northridge earthquake. *J. Geotech. Engng ASCE* **122**, No. 7, 554–564.

Biot, M. A. (1941). General theory of three-dimensional consolidation. *J. Appl. Phys*. **12**, 155–164.

Burke, C., Ling, H. I. & Liu, H. (2004). Seismic response analysis of a full-scale reinforced soil retaining wall. *Proc. 17th ASCE Engineering Mechanics Conf., Newark, DE*.

Calabresi, G., Rampello, S., Sciotti, A. & Amorosi, A. (2000). *Diga sulla Marana Capacciotti: Verifiche delle condizioni di stabilità e analisi del comportamento in condizioni sismiche*. Research Report, University of Roma 'La Sapienza'.

Cascone, E. & Rampello, S. (2003). Decoupled seismic analysis of an earth dam. *Soil Dynam. Earthquake Engng* **23**, No. 5, 349–365.

Chan, A. H. C. (1988). *A unified finite element solution to static and dynamic problems of geomechanics*. PhD thesis, University College of Swansea.

Chan, A. H. C. (1995). *User Manual for DIANA-SWANDYNE II*. School of Engineering, University of Birmingham, UK.

Clough, R. W. & Penzien, J. (1993). *Dynamics of structures*, 2nd edn. New York: McGraw-Hill.

Crespellani, T., Madiai, C. & Vannucchi, G. (1998). Earthquake destructiveness potential factor and slope stability. *Géotechnique* **48**, No. 3, 411–419, **doi**: 10.1680/geot.1998.48.3.411.

Dafalias, Y. F. & Popov, E. P. (1975). A model of nonlinearly hardening materials for complex loading. *Acta Mech*. **21**, No. 3, 173–192.

Dakoulas, P. & Gazetas, G. (2005). Seismic effective-stress analysis of caisson quay walls: application to Kobe. *Soils Found*. **45**, No. 4, 133–147.

Dewoolkar, M. M., Ko, H.-Y. & Pak, R. Y. S. (2001). Seismic behaviour of cantilever retaining walls with liquefiable backfills. *J. Geotech. Geoenviron. Engng ASCE* **127**, No. 5, 424–435.

Elgamal, A.-W. (1992). Three-dimensional seismic analysis of La Villita dam. *J. Geotech. Engng ASCE* **118**, No. 12, 1932–1958.

Elgamal, A.-W., Scott, R. F., Succarieh, M. F. & Liping, Y. (1990). La Villita dam response during five earthquakes including permanent deformations. *J. Geotech. Engng ASCE* **116**, No. 10, 1443–62.

Elgamal, A.-W., Parra, E., Yang, Z. & Adalier, K. (2002). Numerical analysis of embankment foundation liquefaction countermeasures. *J. Earthquake Engng* **6**, No. 4, 447–471.

Elia, G. (2004). *Analisi FEM di problemi al contorno in condizioni statiche e dinamiche con un modello costitutivo avanzato*. PhD thesis, Technical University of Bari, Italy.

Elia, G., Amorosi, A. & Chan, A. H. C. (2004). Nonlinear ground response: effective stress analyses and parametric studies. *Proceedings of the Japan–Europe seismic risk workshop*, Bristol.

Elia, G., Amorosi, A. & Chan, A. H. C. (2005). Fully coupled dynamic analysis of an earth dam using a complex constitutive assumption. *Proc. 11th Int. Conf. of IACMAG, Turin*, 257–264.

Gazetas, G. (1982). Shear vibration of vertically inhomogeneous earth dams. *Int. J. Numer. Anal. Methods Geomech*. **6**, No. 2, 219–241.

Gazetas, G. (1987). Seismic response of earth dams: some recent developments. *Soil Dynam. Earthquake Engng* **6**, No. 1, 2–47.

Gazetas, G. & Dakoulas, P. (1992). Seismic analysis and design of rockfill dams: state-of-the-art. *Soil Dynam. Earthquake Engng* **11**, No. 1, 27–61.

Ghosh, B. & Madabhushi, S. P. G. (2003). A numerical investigation into effects of single and multiple frequency earthquake motions. *Soil Dynam. Earthquake Engng* **23**, No. 8, 691–704.

Griffiths, D. V. & Prevost, J. H. (1988). Two- and three-dimensional dynamic finite element analyses of the Long Valley Dam. *Géotechnique* **38**, No. 3, 367–388, **doi**: 10.1680/geot.1988.38.3.367.

Gruppo di lavoro MPS (2004). *Redazione della mappa di pericolosità sismica prevista dall'Ordinanza PCM 3274 del 20 marzo 2003*. Rapporto conclusivo per il Dipartimento della Protezione Civile, INGV, Milano-Roma.

Hughes, T. J. R. (1983). Analysis of transient algorithms with particular reference to stability behaviour. In *Computational methods for transient analysis* (eds T. Belytschko and T. J. R. Hughes), pp. 67–155. London: Elsevier Science.

Hunter, G. & Fell, R. (2003). Prediction of impending failure of embankments on soft ground. *Can. Geotech. J.* **40**, No. 1, 209–220.

Idriss, I. M. & Sun, J. I. (1992). *SHAKE91: A computer program for conducting equivalent linear seismic response analyses of horizontally layered soils deposits*. Davis, CA: University of California.

Idriss, I. M., Lysmer, J., Hwang, R. & Seed, H.B. (1973). *QUAD-4: A computer program for evaluating the seismic response of soil structures by variable damping finite element procedures*, Report No. EERC 73-16. Berkeley, CA: Earthquake Engineering Research Center, University of California.

Indraratna, B., Balasubramaniam, A. S. & Balachandran, S. (1992). Performance of test embankment constructed to failure on soft marine clay. *J. Geotech. Engng ASCE* **118**, No. 1, 12–33.

Jardine, R. J. & Hight, D. W. (1987). The behaviour and analysis of embankment on soft clay. In *Embankments on soft clays*, pp. 159–244. Athens: Public Works Research Centre.

Jibson, R. W. (1993). Predicting earthquake-induced landslide displacements using Newmark's sliding block analysis. *Transpn Res. Rec.*, No. 1411, 9–17.

Karstunen, M., Krenn, H., Wheeler, S. J., Koskinen, M. & Zentar, R. (2005). Effect of anisotropy and destructuration on the behaviour of Murro test embankment. *Int. J. Geomech*. **5**, No. 2, 87–97.

Karstunen, M., Wiltafsky, C., Krenn, H., Scharinger, F. & Schweiger, H. F. (2006). Modelling the behaviour of an embankment on soft clay with different constitutive models. *Int. J. Numer. Analyt. Methods Geomech*. **30**, No. 10, 953–982.

Katona, M. G. & Zienkiewicz, O. C. (1985). A unified set of single step algorithms. Part 3: The Beta-m method, a generalisation of the Newmark scheme. *Int. J. Numer. Methods Engng* **21**, No. 7, 1345–1359.

Kavvadas, M. & Amorosi, A. (2000). A constitutive model for structured soils. *Géotechnique* **50**, No. 3, 263–273, **doi**: 10.1680/geot.2000.50.3.263.

Kavvadas, M. & Anagnostopoulos, A. (1998). A framework for the mechanical behaviour of structured soils. *Proc. 2nd Int. Symp. on the Geotechnics of Hard Soils–Soft Rocks, Napoli* **2**, 603–614.

Kovacevic, N. (1994). *Numerical analyses of rockfill dams, cut slopes and road embankments*. PhD thesis, University of London.

Krahn, J. (2003). The 2001 R.M. Hardy Lecture: The limits of limit equilibrium analyses. *Can. Geotech. J.* **40**, No. 3, 643–660.

Kwok, A. O. L., Stewart, J. P., Hashash, Y. M. A., Matasovic, N., Pyke, R., Wang, Z. & Yang, Z. (2007). Use of exact solutions of wave propagation problems to guide implementation of nonlinear seismic ground response analysis procedures. *J. Geotech. Geoenviron Engng ASCE* **133**, No. 11, 1385–1398.

Ladd, C. C., Whittle, A. J. & Legaspi, D. E. (1994). Stress-deformation behaviour of an embankment on Boston Blue clay. In *Proceedings of Settlement '94* (eds A. T. Yeung and G. Y. Félio), ASCE Geotechnical Special Publication No. 40, pp. 1730–1759. Reston, VA: ASCE.

Liu, H. & Song, E. (2005). Seismic response of large underground structures in liquefiable soils subjected to horizontal and vertical earthquake excitations. *Comput. Geotech*. **32**, No. 4, 223–244.

Lollino, P., Cotecchia, F., Zdravkovic, L. & Potts, D. M. (2005). Numerical analysis and monitoring of Pappadai dam. *Can. Geotech. J.* **42**, No. 6, 1631–1643.

Madabhushi, S. P. G. & Zeng, X. (2007). Simulating seismic response of cantilever retaining walls. *J. Geotech. Geoenviron. Engng ASCE* **133**, No. 5, 539–549.

Makdisi, F. I. & Seed, B. H. (1978). Simplified procedure for estimating dam and embankment earthquake-induced deformations. *J. Geotech. Engng ASCE* **104**, No. 7, 849–867.

Meng, J. & Rix, G. J. (2003). Reduction of equipment-generated damping in resonant column measurements. *Géotechnique* **53**, No. 5, 503–512, **doi**: 10.1680/geot.2003.53.5.503.

Meroi, E. A., Schrefler, B. A. & Zienkiewicz, O. C. (1995). Large strain static and dynamic semisaturated soil behaviour. *Int. J. Numer. Analyt. Methods Geomech*. **19**, No. 2, 81–106.

Mucciarelli, M. & Gallipoli, M.R. (2006). Comparison between Vs30 and other estimates of site amplification in Italy. *Proc. 1st Eur. Conf. on Earthquake Engineering and Seismology, Geneva*.

Muraleetharan, K. K., Deshpande, S. & Adalier, K. (2004). Dynamic deformations in sand embankments: centrifuge modelling and blind, fully coupled analyses. *Can. Geotech. J.* **41**, No. 1, 48–69.

Naylor, D. J., Maranha, J. R., Maranha das Neves, E. & Veiga Pinto, A. A. (1997). A back-analysis of Beliche Dam. *Géotechnique* **47**, No. 2, 221–233, **doi**: 10.1680/geot.1997.47.2.221.

Newmark, N. M. (1965). Effect of earthquake on dams and embankments. *Géotechnique* **15**, No. 2, 139–160, **doi**: 10.1680/geot.1965.15.2.139.

Özkan, M. Y., Erdik, M., Tunçer, M. A. & Yilmaz, Ç. (1996). An evaluation of Sürgü dam response during 5 May 1986 earthquake. *Soil Dynamics Earthquake Engng* **15**, No. 1, 1–10.

Özkan, M. Y., Özyazicioglu, M. & Aksar, U. D. (2006). An evaluation of Güldürcek dam response during 6 June 2000 Orta earthquake. *Soil Dynamics Earthquake Engng* **26**, No. 5, 405–419.

Pagano, L., Desideri, A. & Vinale, F. (1998). Interpreting the settlement profiles of earth dams. *J. Geotech. Geoenviron. Engng ASCE* **124**, No. 10, 923–932.

Pagano, L., Sica, S. & Desideri, A. (2006). Representativeness of measurements in the interpretation of earth dam behaviour. *Can. Geotech. J.* **43**, No. 1, 87–99.

Paoliani, P. (2001). The behaviour of Acciano earth dam during the Umbria-Marche earthquake of September 1997. *Riv. Ital. Geotec*. **2**, 20–27.

Pastor, M., Zienkiewicz, O. C. & Chan, A. H. C. (1990). Generalized plasticity and the modelling of soil behaviour. *Int. J. Numer. Analyt. Methods Geomech*. **14**, No. 3, 151–190.

Penman, A. D. M. (1986). On the embankment dam. *Géotechnique* **36**, No. 3, 303–348, **doi**: 10.1680/geot.1986.36.3.303.

Poulos, H. G., Booker, J. R. & Ring, G. J. (1972). Simplified calculation of embankment deformations. *Soils Found*. **12**, No. 4, 1–17.

Prato, C. A. & Delmastro, E. (1987). 1-D seismic analysis of embankment dams. *J. Geotech. Engng ASCE* **113**, No. 8, 904–909.

Prevost, J. H. (1978). Plasticity theory for soil stress–strain behaviour. *J. Engng Mech. ASCE* **104**, No. 5, 1177–1194.

Prevost, J. H., Abdel-Ghaffar, A. M. & Elgamal, A.-W. (1985). Nonlinear hysteretic dynamic response of soil systems. *J. Engng Mech. ASCE* **111**, No. 7, 882–897.

Ramalho-Ortigão, J. A., Werneck, M. L. G. & Lacerda, W. A. (1983). Embankment failure on clay near Rio de Janeiro. *J. Geotech. Engng ASCE* **109**, No. 11, 1460–1479.

Rathje, E. M. & Bray, J. D. (2000). Nonlinear coupled seismic sliding analysis of earth structures. *J. Geotech. Geoenviron. Engng ASCE* **126**, No. 11, 1002–1014.

Rouainia, M. & Muir Wood, D. (2000). A kinematic hardening constitutive model for natural clays with loss of structure. *Géotechnique* **50**, No. 2, 153–164, **doi**: 10.1680/geot.2000.50.2.153.

Schnabel, P. B., Lysmer, J. & Seed, H. B. (1972). *SHAKE: a computer program for earthquake response analysis of horizontally layered sites*, Report No. EERC 72–12. Berkeley, CA: Earthquake Engineering Research Center, University of California.

Seed, H. B. (1980). Lessons from the performance of earth dams during earthquakes. In *Design of dams to resist earthquakes*, pp. 251–258. London: Institution of Civil Engineers.

Seed, H. B., Murarka, J., Lysmer, J. & Idriss, I. M. (1976). Relationships between maximum acceleration, maximum velocity, distance from source and local site conditions for moderately strong earthquakes. *Bull. Seismol. Soc. Am*. **66**, No. 4, 1323–1342.

Seed, H. B., Seed, R. B., Lai, S. S. & Khamenehpour, B. (1985). Seismic design of concrete faced rockfill dams. In *Concrete face rockfill dams: Design, construction and performance* (eds J. B. Cooke and J. L. Sherard), pp. 459–478. New York: ASCE.

Sica, S., Pagano, L. & Modaressi, A. (2008). Influence of past loading history on the seismic response of earth dams. *Comput. Geotech*. **35**, No. 1, 61–85.

Tavenas, F. & Leroueil, S. (1980). The behaviour of embankments on clay foundations. *Can. Geotech. J.* **17**, No. 2, 236–260.

Vucetic, M. & Dobry, R. (1991). Effects of the soil plasticity on cyclic response. *J. Geotech. Engng ASCE* **117**, No. 1, 89–107.

Wieland, M. & Malla, S. (2002). Seismic safety evaluation of a 117 m high embankment dam resting on a thick soil layer. *Proc. 12th Eur. Conf. on Earthquake Engng, London*.

Woodward, P. K. & Griffiths, D. V. (1996). Influence of viscous damping in the dynamic analysis of an earth dam using simple constitutive models. *Comput. Geotech*., **19**, No. 3, 245–263.

Zdravkovic, L., Potts, D. M. & High, D. W. (2002). The effect of strength anisotropy on the behaviour of embankments on soft ground. *Géotechnique* **52**, No. 6, 447–457, **doi**: 10.1680/geot.2002.52.6.447.

Zienkiewicz, O. C., Chan, A. H. C., Pastor, M., Schrefler, B. A. & Shiomi, T. (1999). *Computational geomechanics (with special reference to earthquake engineering)*. Chichester: John Wiley & Sons.